PROCEEDINGS OF THE ROYAL SOCIETY B

Proc. R. Soc. B (2010) **277**, 3579–3586
doi:10.1098/rspb.2010.0509
Published online 23 June 2010

The craniomandibular mechanics of being human

Stephen Wroe[1,*], Toni L. Ferrara[1], Colin R. McHenry[1,2], Darren Curnoe[1] and Uphar Chamoli[1]

[1]*Computational Biomechanics Research Group, Evolution and Ecology Research Centre, School of Biological, Earth and Environmental Sciences, University of New South Wales, Sydney, NSW 2052, Australia*
[2]*School of Engineering, University of Newcastle, NSW 2308, Australia*

Diminished bite force has been considered a defining feature of modern *Homo sapiens*, an interpretation inferred from the application of two-dimensional lever mechanics and the relative gracility of the human masticatory musculature and skull. This conclusion has various implications with regard to the evolution of human feeding behaviour. However, human dental anatomy suggests a capacity to withstand high loads and two-dimensional lever models greatly simplify muscle architecture, yielding less accurate results than three-dimensional modelling using multiple lines of action. Here, to our knowledge, in the most comprehensive three-dimensional finite element analysis performed to date for any taxon, we ask whether the traditional view that the bite of *H. sapiens* is weak and the skull too gracile to sustain high bite forces is supported. We further introduce a new method for reconstructing incomplete fossil material. Our findings show that the human masticatory apparatus is highly efficient, capable of producing a relatively powerful bite using low muscle forces. Thus, relative to other members of the superfamily Hominoidea, humans can achieve relatively high bite forces, while overall stresses are reduced. Our findings resolve apparently discordant lines of evidence, i.e. the presence of teeth well adapted to sustain high loads within a lightweight cranium and mandible.

Keywords: form and function; Hominoidea; fossil

1. INTRODUCTION

The widely held view that anatomically modern *Homo sapiens* can neither generate nor withstand high bite forces is based on evidence for more powerful masticatory musculatures and more robust skull architectures in other members of the family Hominidae (systematic nomenclature given in §2), as well as predictions using two-dimensional lever models (Walker 1981; Demes & Creel 1988). This conclusion implies that our species either adapted to eat less hard/tough foods, or developed behaviours that facilitated extra-oral processing (Wrangham *et al.* 1999). Reduction of jaw muscle mass has even been proposed as a prerequisite for increased brain size in *Homo* (Stedman *et al.* 2004; McCollum *et al.* 2006).

There are, however, reasons to question this traditional interpretation of human cranial mechanics. Published mean maximal bite force data for *H. sapiens* vary greatly (Waugh 1937; Pruim *et al.* 1980; Sinn *et al.* 1996) and are mostly based on modern western populations, as opposed to hunter–gatherers, who may be more appropriate subjects in the context of understanding human evolution. Direct bite force data for comparison is unavailable for all other hominoid species. Moreover, the modern human dentition appears well adapted to sustain high loads, being characterized by large tooth root surface areas and tooth enamel that is relatively thicker than in any other extant hominid (Kupczik & Dean 2008; Olejniczak *et al.* 2008; Vogel *et al.* 2008). These features are widely considered to be indicators of both a capacity to resist high loadings and dietary preference (Olejniczak *et al.* 2008; Vogel *et al.* 2008). Consequently, within conventional interpretations, the presence of thick tooth enamel and large tooth root surface areas in modern humans are explained as plesiomorphies that have been retained, whereas other associated features of the masticatory apparatus have been reduced (Kupczik & Dean 2008).

The argument that the bite of *H. sapiens* is relatively weak is based primarily on two-dimensional lever mechanics, wherein muscle forces are reduced to single vectors for each major muscle group. This results in greatly simplified representation of the musculature, which in reality originates and inserts across broad areas. Although this method has proved a very useful heuristic tool in comparative studies for a range of taxa (Thomason *et al.* 1990; Thomason 1991; Wroe *et al.* 2005; Christiansen & Wroe 2007), it cannot account for the combined effects of torque produced by complex arrangements of muscle fibres over broad areas (Rohrle & Pullan 2007; Davis *et al.* 2010). The use of single force vectors to approximate major muscle groups can greatly underestimate (Thomason 1991; Rohrle & Pullan 2007; Ellis *et al.* 2008) and sometimes overestimate (McHenry *et al.* 2007) bite reaction forces. This method is further limited in that it cannot shed light on stress–strain distributions, and is therefore ill suited to evaluating the ability of anatomical structures to sustain predicted forces.

Here, using three-dimensional finite element analysis (FEA), we test the hypothesis that the human bite is weak and the skull unable to sustain high bite forces compared with that of other hominoids. Our approach allows much more accurate simulation of muscle architecture as

* Author for correspondence (s.wroe@unsw.edu.au).

Electronic supplementary material is available at http://dx.doi.org/10.1098/rspb.2010.0509 or via http://rspb.royalsocietypublishing.org.

Received 9 March 2010
Accepted 3 June 2010

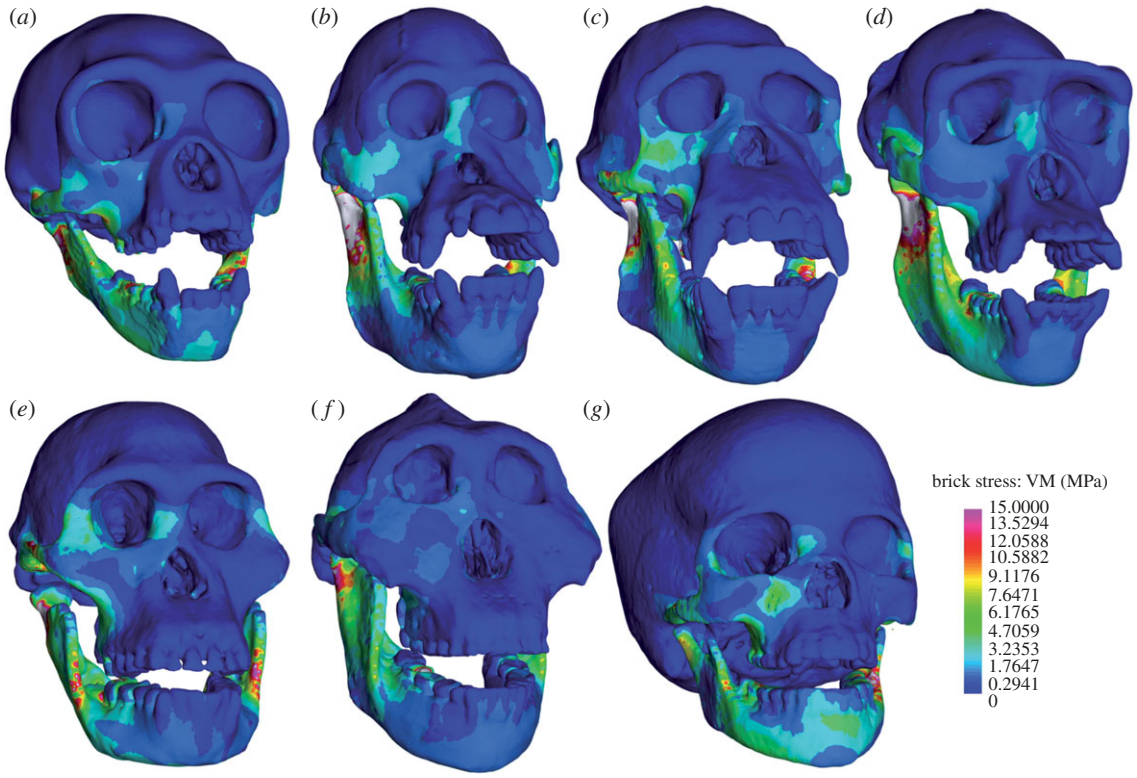

Figure 1. Visual plots of von Mises (VM) stress distributions in finite element models scaled to a uniform surface area and bite force simulating unilateral bites at the second molar: (*a*) *Hylobates lar*; (*b*) *Pongo pygmaeus*; (*c*) *Pan troglodytes*; (*d*) *Gorilla gorilla*; (*e*) *Australopithecus africanus*; (*f*) *Paranthropus boisei*; (*g*) *Homo sapiens*. Dark blue regions show no or minimal stress with stress increasing to 15 MPa in pink regions. Highest stresses are in white regions, i.e. greater than 15 MPa.

well as predictions of stress–strain magnitudes and distributions (Rayfield *et al.* 2001; Preuschoft & Witzel 2005; McHenry *et al.* 2007; Wroe *et al.* 2007*b*; Strait *et al.* 2009). Results are based on the analyses of finite element models (FEMs) of complete crania and mandibles generated from computerized tomography (CT). Models for FEMs comprise crania and mandibles of five extant members of the Hominoidea: *H. sapiens*, *Pan troglodytes* (common chimpanzee), *Gorilla gorilla* (gorilla), *Pongo pygmaeus* (orangutan) and *Hylobates lar* (white-handed gibbon), and two fossil hominins, *Australopithecus africanus* and *Paranthropus boisei* (figure 1). We also constructed a further FEM for a specimen of *Macaca fascicularis*, previously modelled by Kupczik *et al.* (2007). Results generated in the analysis of our FEM of this specimen were compared with both experimental and FEA data provided by Kupczik *et al.* (2007) in order to examine the effectiveness of our approach.

2. MATERIAL AND METHODS

Systematic nomenclature follows Wood & Richmond (2000), wherein Hominoidea comprises Hylobatidae and Hominidae (great apes, including *Homo*). The term 'hominine' is inclusive of the common ancestor of *Pan* and *Homo* and 'hominin' refers to bipedal great apes only.

(a) *Model pre-processing*

FEMs of extant specimens are based on adult females. The *H. sapiens* skull is that of a San hunter–gatherer. The fossil hominins probably represent sub-adult and adult males, respectively (and see the electronic supplementary material). All FEMs comprise tet4 elements assigned a homogeneous material property set with a Young's modulus of elasticity of 14 GPa and a Poisson's ratio of 0.3 for bone. These values gave the closest approximations to experimental readings in previous validation of a *M. fascicularis* specimen (Kupczik *et al.* 2007) that has been reassembled from original CT in the present study (see figure 3 and the electronic supplementary material). Few data are available regarding material properties for extant hominoids and none for fossil species. Furthermore, the assignment of multiple material properties to incomplete fossil specimens, particularly *P. boisei*, would necessitate the introduction of further assumptions. Differences in the distribution of materials can influence the results (Strait *et al.* 2005; McHenry *et al.* 2007; Wroe *et al.* 2007*b*). Our methods enable investigation of the role of geometry, which is fundamental to mechanical performance, but they are not intended to predict absolute stress–strain magnitudes. This comparative approach, widely applied in biological FEA, centres on the assessment of relative rather than absolute performance (Rayfield 2005; McHenry *et al.* 2007; Wroe *et al.* 2007*a*; Dumont *et al.* 2009). Increased precision regarding properties will lead to more accurate predictions of actual stress–strain magnitudes, but previous work suggests that neither general stress–strain patterns nor bite forces are greatly affected by varying material properties (McHenry *et al.* 2007; Wroe *et al.* 2007*b*; Strait *et al.* 2009).

For all FEMs, segmentation was performed using Mimics (v. 12.02) and solid modelling in Strand7 (v. 2.3) largely following previously published protocols (McHenry *et al.* 2007; Wroe *et al.* 2007*b*, 2008; Bourke *et al.* 2008; Clausen *et al.* 2008; Wroe 2008). Element number and specimen data, respectively, for extant species were as follows: *H. sapiens* (953902, NMB 1271); *P. troglodytes* (1224778, USNM

395820); *G. gorilla* (1213134, AM 37431); *P. pygmaeus* (971774, NMV C26885); and *H. lar* (1049590, NMV C2909). Element numbers for fossil species were 1046435 for *A. africanus* and 1126317 for *P. boisei*. For extant material, CT was performed at the Mater Hospital, Newcastle, using a Toshiba Aquilion 16 scanner. CT data for fossil material (Sts 5; Broom 1947) and OH 5; Leakey 1959)) were purchased through http://www.virtualanthropology.com/3d_data/3d-archive.

Muscle forces, provided in the electronic supplementary material, were predicted using estimates of cross-sectional area following O'Connor *et al.* (2005). Here, muscles were reconstructed as multiple pre-tensioned trusses, using a method that facilitates a more realistic spread of forces and much closer approximations of three-dimensional muscle geometry than can be achieved using single vectors (McHenry *et al.* 2007; Wroe *et al.* 2007*a*; figure 2).

(b) *Virtual reconstruction of fossil material*

Reconstruction of the cranium of *A. africanus* is based on CT of Sts 5, but with the upper dentition and mandible from research casts of Sts 52. Our model of *P. boisei* is based on OH 5 and a research cast of the mandible NMT-W64-160. Missing anatomy has been reconstructed by warping a half surface mesh of *P. troglodytes* to fit the geometry of the fossil taxa and using this to replace missing regions in original specimens. As the fossil hominin mandibles and dentition are based on casts, for these two specimens, these elements are modelled as solid bone without vacuities. Thus, the two reconstructed fossil mandibles provide three-dimensional bases for jaw muscle insertions, but surface stresses are likely to be underestimates relative to those in the FEMs of the five extant species, wherein vacuities have been incorporated.

Where present, we removed matrix from the orbits and sinuses, as well as the nasal and endocranial cavities using segmentation tools in Mimics (v. 12.02). Internal cranial geometry missing in both fossil hominins (posterior naso-pharynx of Sts 5, anterior neurocranium and sphenoid of OH 5) were reconstructed by deforming the intact mesh from the *P. troglodytes* model. Mesh deformation was achieved through a series of two-dimensional grid warps in sagittal, coronal and transverse planes—a pseudo-three-dimensional version of D'Arcy Thompson transformation grids (Thompson 1917).

For both fossils, a half-cranium of a *P. troglodytes* surface mesh was aligned and scaled (by basal skull length) to the fossil half-skull in a three-dimensional Computer-Assisted Design application (RHINO v. 4). Equivalent slices of the *P. troglodytes* and fossil mesh, superimposed upon a grid, were exported as bitmaps to a two-dimensional graphics application (Paintshop Pro v. 8). Each slice of the *Pan* surface mesh was deformed to match the geometry of the equivalent slice of the fossil mesh, using the 'Mesh Warp' tool (figure 1 and electronic supplementary material, S1). The geometry preserved in the fossil 'slice' provided a template for deforming the geometry of the *Pan* 'slice'. Using the lowest possible resolution of the Mesh Warp tool maximized the influence of this process upon geometry (of the *P. troglodytes* mesh) that was not preserved in the fossil. Thus, those parts of the *P. troglodytes* mesh corresponding with the missing portions of the fossil were deformed by the weighted sum of the deformations imposed upon nearby geometry, the latter corresponding to structures that were preserved in the fossil.

The warping of each slice of the *P. troglodytes* surface mesh produced a warped grid that recorded the deformations required for that two-dimensional slice. Those deformations were then replicated on the respective slice of the three-dimensional *P. troglodytes* half-skull mesh using a three-dimensional grid-based mesh deformation tool in RHINO. Repeating this process in multiple sagittal, coronal and then transverse slices gave the required deformations for each node in the three-dimensional grid. This approach alters both the internal and external surfaces of

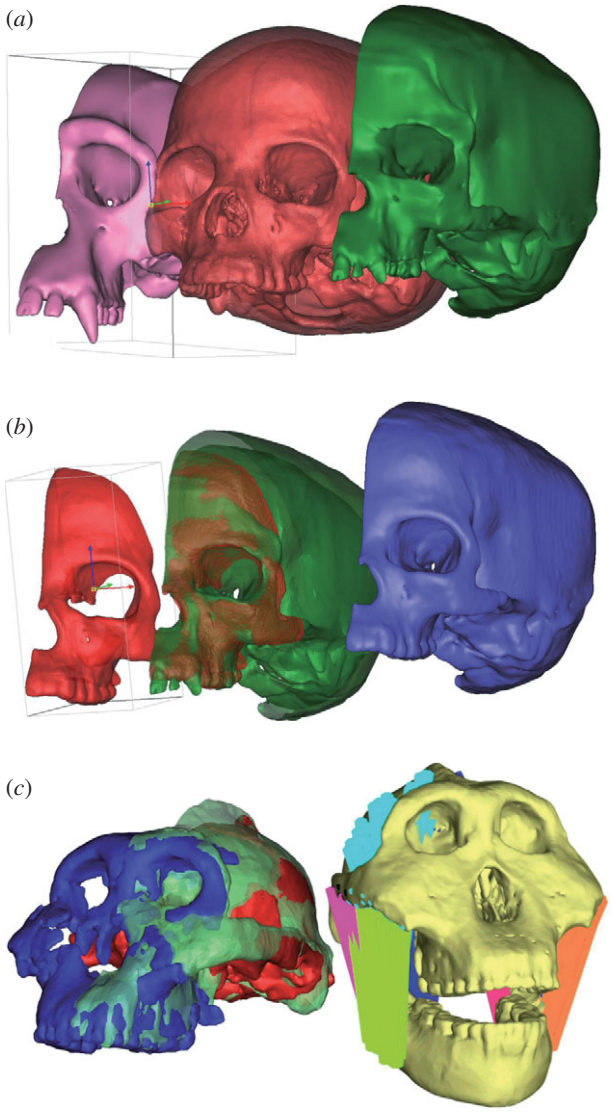

Figure 2. Reconstruction. (*a*) To test protocols for reconstructing missing data in fossil skulls a left-side half cranial mesh of *P. troglodytes* (pink) was warped to fit the left side of a cranial mesh of a *H. sapiens* (red) to produce a deformed *Pan* mesh (green). (*b*) The left facial region of the original *H. sapiens* mesh was isolated and internal geometry removed (red). This was merged with the deformed *Pan* to produce a new '*H. sapiens*' mesh (blue) in which approximately 85% of original *H. sapiens* geometry was replaced by the deformed *Pan*. Performance of a finite element model (FEM) based on this reconstructed half cranial mesh was compared with that of a half cranial FEM generated from the original *H. sapiens* data. Under equivalent loadings, stress distributions were almost identical in both FEMs (see electronic supplementary material). (*c*) Meshes of *P. boisei* facial skeleton (blue) and posterior cranium (red) superimposed on half-cranial mesh warped from an STL of *P. troglodytes* to fit fossil material (green); and FEM of *P. boisei* with muscles modelled as pre-tensioned truss elements.

the *Pan* mesh to provide an approximation of the missing portions of the fossil mesh. The internal geometry of the deformed *P. troglodytes* mesh, corresponding to the missing portions of the fossil, were then merged with the three-dimensional data from the fossils to produce an intact half-mesh based upon each fossil. Half-meshes were then mirrored to produce whole crania.

Sts 5 (*A. africanus*): surface mesh deformation was concentrated upon the facial skeleton, the region of Sts 5 showing the poorest preservation. Consequently, a single iteration was considered sufficient for deforming the *P. troglodytes* mesh (electronic supplementary material, table S1). Only geometry from the left half of the cranial meshes was considered. Deformation grids were produced for three sagittal slices, three coronal slices and nine transverse slices, giving a total of 1608 nodes in the resulting three-dimensional grids that were used to deform the *Pan* mesh within RHINO.

OH 5 (*P. boisei*): as the missing portion of this specimen includes the anterior neurocranium and the sphenoid region of the posterior palate and basicranium, the deformation of the *P. troglodytes* mesh involved an entire half-skull (left side). Target geometry for the deformation was created by mirroring the right side of OH 5 and adding this to the preserved left side of the fossil. Data from a research cast of OH 5, which includes reconstruction of the missing portions was also incorporated into the target geometry. During deformation of the *P. troglodytes* mesh, the geometry of the internal and external surfaces of the fossil material was used as primary data, with the geometry of the external surface of the cast as a secondary guide.

Two iterations of the mesh deformation process were used, as the whole of the half-cranium was being deformed. In the first iteration, a small number of low-resolution (20 mm) grids were used to derive a first approximation of overall geometry: this was refined in a second iteration using a larger number of 10 mm and 5 mm grids (electronic supplementary material, table S1). The nodes in the resulting three-dimensional grids used to deform the chimpanzee surface mesh within RHINO totalled 1338 for the first iteration and 22 650 for the second.

(c) *Sensitivity analyses and test of protocols*

To gauge the accuracy of our reconstruction protocols, two additional FEMs were generated: an unaltered half-model of the original *H. sapiens* cranium and a half-model, wherein approximately 85 per cent was replaced using a surface mesh of *P. troglodytes* warped to fit the human specimen (see figure 2 and the electronic supplementary material). The left side of the *P. troglodytes* cranial mesh was deformed to the corresponding geometry of the left side of the *H. sapiens* mesh as described above. Because of the large differences in neurocranial morphology between these two surface meshes, two iterations of sagittal-plane deformations were used (electronic supplementary material, table S1). This resulted in a deformed *P. troglodytes* mesh with a strong superficial resemblance to the *H. sapiens* mesh (figure 2).

Approximately 85 per cent of the original human mesh was then removed. This included all internal and external regions posterior to the postorbital bar and a further internal cylindrical section (length 25 mm, diameter 36 mm) of the naso-pharynx. The deformed *P. troglodytes* mesh was used to replace this entire section, such that only around 15 per cent of the final reconstructed *H. sapiens* mesh was based on the original *H. sapiens* material, the remaining 85 per cent being comprised entirely of the warped *P. troglodytes* mesh.

FEMs of both the original and reconstructed *H. sapiens* half models were produced in Strand7 (v. 2.3) with material properties assigned as in the previous hominid models. These two FEMs were constrained at the canines and occipital condyles, and in translation on the 'cut' surfaces. Equivalent loadings were applied to the zygomatic arches of both. Despite the great majority of its cranial geometry having been replaced by the deformed *P. troglodytes* mesh, von Mises (VM) stress distributions in the reconstructed *H. sapiens* model were very similar to those observed in the model based entirely on the original *H. sapiens* CT (electronic supplementary material, figure S2). We have used VM stress as an indicator of mechanical performance in this study because it is a good indicator of mechanical performance in materials that fail under a ductile model of fracture (Nalla *et al.* 2003; Dumont *et al.* 2005).

An additional FEM based on CT of *M. fascicularis*, the focus of previous investigation (Kupczik *et al.* 2007), was also assembled to examine the efficacy of our methods. Applying our protocols for FEM generation and previously applied boundary conditions, provides results which are largely in agreement with experimentally derived findings (Kupczik *et al.* 2007). See electronic supplementary material for more detailed comparison.

(d) *Load cases*

Three separate sets of linear static simulations were solved for each species: (i) specimen-specific estimated muscle forces were applied to unscaled models to predict actual performance; (ii) in order to examine the influence of size differences between specimens and to quantify differences in efficiency, analyses were run with models rescaled to the total surface area of the *P. troglodytes* FEM and uniform muscle forces applied (Dumont *et al.* 2009); and (iii) a final set of simulations was solved for each of these scaled models to determine how well-adapted each species was to withstand the stresses generated in the production of a given bite reaction force. In this third set of simulations, muscle forces were adjusted to achieve the same bite reaction force in all scaled models. Temporomandibular joint (TMJ) reaction forces were also taken from the FEMs (Clausen *et al.* 2008; and see the electronic supplementary material).

For each of the above simulations, we applied loads simulating maximum unilateral bites at the canine, second premolar and second molar, respectively. Our aim was to assess relative peak performances. Typically, not all muscle groups are recruited maximally or simultaneously during mastication and relative inputs from working and balancing sides vary (Hylander *et al.* 1992). Work on other taxa shows that maximal involuntary bite forces can greatly exceed those recorded voluntarily by approximately 40–60% (Ellis *et al.* 2008). Mammals generally avoid damage to their teeth and jaws through sensory feedback (Lund & Kolta 2006), but tooth breakage is not uncommon (Wroe *et al.* 2007*b*). Muscle forces applied to unscaled models therefore represent theoretical maxima unlikely to be achieved under normal conditions.

3. RESULTS

Muscle forces calculated for humans are close to an average previously predicted for *H. sapiens* using the same

approach, wherein cross-sectional areas were likewise calculated for material that represented a range of hunter–gatherers (O'Connor *et al.* 2005). These forces are less than two-thirds that estimated for *P. boisei* and less than half that of *P. troglodytes* (see electronic supplementary material). For most species, our estimates are similar to or higher than those previously predicted using another, similar method (Demes & Creel 1988). Further simulations of the human FEM were run applying the still lower average muscle forces for a female human presented by Demes & Creel (1988), and see figure 3*a*.

For unscaled models, the highest bite forces in Newtons (N) were obtained at the second molar from *P. boisei* (2161 N), followed by *G. gorilla* (1723 N), *P. troglodytes* (1511 N), *H. sapiens* (1109 N or 1317 N and see below), *P. pygmaeus* (1031 N), *A. africanus* (831 N) and *H. lar* (136 N).

We found that bite force was broadly proportional to body mass (as predicted using a method based on cranial data that provides body mass estimates most comparable to those generated on the basis of postcranial reconstructions (Aiello & Wood 1994)). Predicted body masses for the hominid specimens ranged from 30.6 kg for *A. africanus* to 127.5 kg for *G. gorilla*. The relationship between bite force and body mass showed slightly positive or near-positive allometry, depending on bite point (see electronic supplementary material, figure S5). Relative to predicted body masses, *P. boisei* (67 kg) generated the highest bite forces and *G. gorilla* the lowest.

Whether we used ours or the lower muscle forces of Demes & Creel (1988), comparison of results from unscaled FEMs (figure 3) shows that maximum bite forces in the humans are close to those that would be expected on the basis of body mass for a hominoid (electronic supplementary material, figure S5), being intermediate between those for the smaller *P. pygmaeus* (body mass 37.4 kg) and a *P. troglodytes* of higher body mass (49.9 kg). Our estimates for theoretical maximum bite forces in *H. sapiens* exceed mean values obtained for voluntary bite force taken from modern western populations (365 N; Sinn *et al.* 1996; to 965 N; Pruim *et al.* 1980), but are close to the mean for the only published data available for a hunter–gatherer population, a large sample of Inuit (1235 N; Waugh 1937). No direct data were available for other taxa. Maximum bite forces as high as 2000 N have been indirectly inferred for *P. pygmaeus* (Lucas *et al.* 1994), considerably higher than predicted by our FEM. However, our specimen was from a young-adult female, considerably smaller than the *H. sapiens* and less than one-third of the predicted body mass of the female *G. gorilla* included in the study. It is probable that modelling of larger female and male *P. pygmaeus* would yield considerably higher bite forces.

In unscaled simulations, mean stresses are relatively low in the cranium of *H. sapiens*, but higher in the mandible than for other taxa, except *H. lar* (figure 4). Results from FEMs uniformly scaled to the same total skull surface area and muscle force demonstrate that, at 2146 N, the human would produce a much greater bite force than any other hominid, quantifying and confirming the relative efficiency of the human masticatory apparatus (figure 3). Thus, when each of the skulls is scaled to the same total surface area and the muscle forces predicted

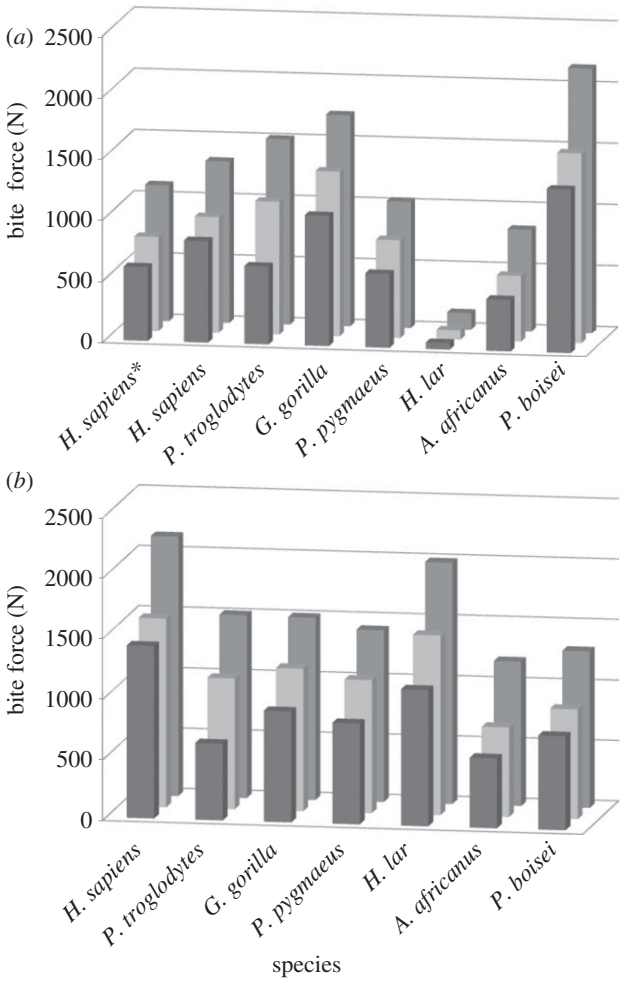

Figure 3. Bite forces (N, Newtons) in unilateral bites at the canine, second premolar and second molar. (*a*) Unscaled finite element models (FEMs). We note that there are considerable differences in the estimated body mass between specimens, for example the *G. gorilla* is more than 3.4 times the body mass of the *P. pygmaeus*, and 1.8 times the body mass of OH 5. (*b*) FEMs scaled to the surface area of *P. troglodytes* with uniform muscle forces applied. Asterisk (*) denotes muscle forces for *H. sapiens* taken from Demes & Creel (1988). Black bars, canine; light grey bars, premolar; dark grey bars, molar.

for *P. troglodytes* are also applied to each, the human's bite is at least 42 per cent higher than all other taxa excepting the hylobatid, *H. lar*, which approaches the human in terms of efficiency. However, high stresses would develop in both the human and hylobatid skulls under such hypothetical loadings (figure 4). In simulations, wherein all FEMs are scaled to a uniform surface area and bite force (1511 N), mean stresses are relatively low in the cranium of *H. sapiens*, but still higher in the mandible than for other hominids.

Mean stresses are only approximate guides to performance. High localized stresses, indicating regions that are more likely to fail may be apparent in structures that record low mean values. Whether or not a structure is more resistant to failure is probably a more meaningful indicator of mechanical performance. Bone fails under a ductile model of fracture (Nalla *et al.* 2003) and VM stress has been considered a good predictor of failure

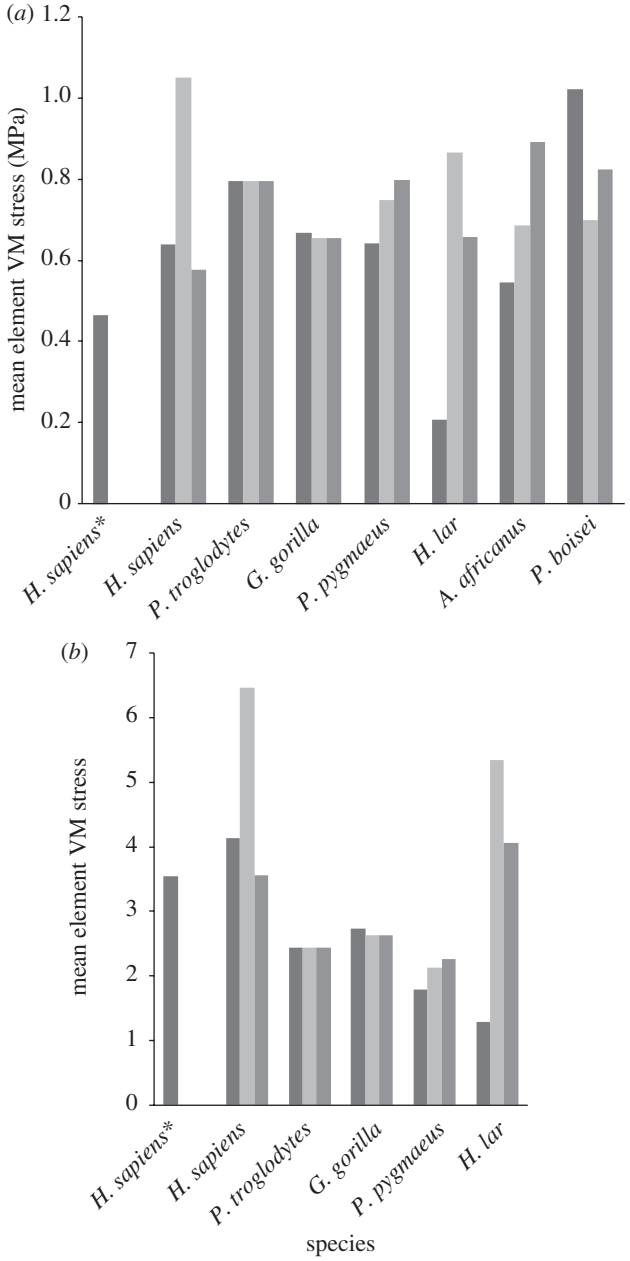

Figure 4. Mean element VM stress (in megapascals) in unilateral bites at the second molar for finite element models that are 1, unscaled; 2, scaled to the surface area and muscle forces of *P. troglodytes*; and, 3, scaled to the surface area and bite force of *P. troglodytes*. (*a*) Cranium; (*b*) mandible. Black bars, unscaled; light grey bars, scaled to muscle force; dark grey bars, scaled to bite force.

under ductile fracture (Dumont *et al.* 2005). The location of peak VM stresses can predict the point of failure in vertebrate bone even where homogeneous material properties are assumed (Tsafnat & Wroe in press), although this has yet to be demonstrated in a wide variety of structures and taxa. More work is needed to better determine the effectiveness of VM stress and other indicators as predictors of material failure in bone.

In visual plots of FEMs scaled to uniform skull surface area and bite force (figure 1), the human cranium shows less extensive and lower magnitudes of stress than *P. troglodytes*, but clearly more extensive and higher peak stresses than *P. boisei* and *G. gorilla*. However, in all species the highest stresses are not generated in the crania, but in the mandibles. This also applies to the two fossil hominids for which mandibles were modelled as solid bone. Thus, our results suggest that in all taxa, the mandible may be more susceptible to failure than the cranium, and the highest stresses recorded in any of these FEMs (shown in white) are in the mandibles of *G. gorilla*, *P. pygmaeus* and *P. troglodytes*, where the condylar neck reveals stresses in excess of 15 MPa. Whether or not peak stresses are actually lower in the mandibles of *P. boisei* and *A. africanus* than in these three extant great apes will require modelling of the fossil mandibles with internal vacuities, rather than as solid structures (which are likely to underestimate predicted surface stresses relative to the mandibles of the other taxa).

Importantly, these peak stresses in the condylar neck are much lower in the *H. sapiens* FEM than for all other hominids when models are scaled to the same bite force and total surface area (figure 1). Among extant hominoids, the distributions and magnitudes of stress in the human mandible are most similar to those generated in the mandible of *H. lar*.

4. DISCUSSION AND CONCLUSION

Our results show that the human can produce bite forces comparable to those of similar-sized extant hominids while applying considerably less muscular force from the jaw adductors. The question that then arises is whether the human cranium and mandible are well adapted to withstand such forces. Although comparisons of results from simulations of models scaled to the same bite force and total surface area indicate that the crania of *G. gorilla* and *P. boisei* are less stressed than those of other taxa, as shown in both visual plots (figure 1) and mean element stress data (figure 4), neither peak nor mean stress data suggest that the human crania is clearly more stressed than those of the remaining four hominoid species considered here (figures 1 and 4).

Results showing that the highest peak and mean stresses in the hominoid mandible under all load cases, are consistent with the argument that the vertebrate mandible may provide more direct indications of anatomical adaptation to feeding behaviour than the cranium (Preuschoft & Witzel 2002). This may be because the form of the mandible is less influenced by the need to serve other functions not related to the mechanical processing of food, such as housing and protecting neural and sensory organs (Thomason 1991; Preuschoft & Witzel 2002). Although mean stresses are relatively high in the human mandible when adjusted to the same surface area and bite force, these are better distributed in *H. sapiens* and peak stresses are lower than in all other taxa. We conclude that because peak stresses are lower, the human mandible may in fact be better adapted than those of other hominids to resist stresses developed under the specific loadings applied here, which are designed to simulate peak transitory bite forces.

Our findings offer an explanation for the apparently inconsistent presence of a dentition in *H. sapiens* that appears well adapted to resist high bite forces relative to other extant hominids, set in a cranium and mandible that are relatively gracile and characterized by less robust musculature. Thus, the teeth of humans need to

be able to resist comparable bite reaction forces to those of other extant hominids, but, because considerably less muscle force is required to achieve any given bite reaction force in the human than in other hominids, less stress is produced. Consequently, the overall structure required to sustain these forces need not be as robust. Likewise, our results demonstrate high efficiency in the bite of *H. lar*, offering an explanation for the presence of thick tooth enamel in another hominoid characterized by a relatively gracile skull and jaw-closing musculature.

The relative efficiency of the masticatory apparatus in *H. sapiens* and *H. lar* is most probably explained by several factors, the most important in the context of the present study being the effective three-dimensional arrangement of jaw closing muscles, features which cannot be accurately simulated in two-dimensional models, or even three-dimensional models, wherein lines of action for muscle major groups are reduced to single force vectors (Rohrle & Pullan 2007; Davis *et al.* 2010). Compared with three-dimensional modelling, two-dimensional techniques tend to over-estimate torque produced by the masseter and underestimate that produced by the temporalis (Davis *et al.* 2010). The shorter outlever (the distance between the TMJ and bite point), incorporating the reduced distances between the TMJ and the occlusal plane, is undoubtedly an important factor in the increased efficiency of biting, which allows high bite forces to be developed even though muscle-generated forces are reduced. Lower overall muscle forces, and altered muscle-force vectors resulting from the shortening of the jaw and the decrease in mandibular depth, are expected to reduce joint reaction forces (Smith & Savage 1959; Taylor 2005). Although our models do not explicitly test which morphological features are responsible for differences in bite and joint reaction forces, relatively low TMJ reaction forces in our human FEM are consistent with this proposition when scaled to the same total surface area and bite force as other taxa.

Considered together with tooth anatomy, our results indicate that relative to other hominids, the capacity of modern humans to crack hard objects has been underestimated. This may impact on how we interpret the evolution of human feeding behaviour, but does not mean that changes in our masticatory apparatus have not otherwise limited food processing capacity. The higher mandibular rami of other hominids may reduce effectiveness of the temporalis when rotating the mandible about the transverse axis. However, during sustained chewing, which involves lateral or anteroposterior mandibular translation, the role of the temporalis is secondary to those of the masseteric and pterygoid musculature (Smith & Savage 1959). A TMJ positioned further above the occlusal plane may provide greater area for muscle attachment for masseteric and pterygoid musculature, as well as a more even spread of occlusal forces (Taylor 2005), and there is strong correlation between ramus height and the degree of translation in anthropoid primates (Wall 1999). We conclude that although humans are well adapted to produce high peak forces with the jaw moving in rotation, they may not be as well adapted to produce and maintain high bite forces with the jaw moving in translation. Thus, *Homo sapiens* may be comparable to other hominids in possessing an ability to access some relatively hard foods through the application of high transitory bite forces, however, our species may be less well adapted to consume tough or hard foods that require powerful, sustained chewing.

Work was funded by ARC (DP0666374, DP0987985, DP0986471), UNSW Internal Strategic Initiatives grants and U. Newcastle DVCR funding to S.W. and C.R.M. We thank K. Kupczik for the provision of CT and load data, A. Walker for assistance in muscle reconstruction for *P. boisei*, E. Cunningham (Mater Hospital) for CT and S. Ingelby (Australian Museum) for access to specimens.

REFERENCES

Aiello, C. L. & Wood, B. A. 1994 Cranial variables as predictors of hominine body mass. *Am. J. Phys. Anthropol.* **95**, 409–426. (doi:10.1002/ajpa.1330950405)

Bourke, J., Wroe, S., Moreno, K., McHenry, C. & Clausen, P. 2008 Effects of gape and tooth position on bite force and skull stress in the dingo (*Canis lupus dingo*) using a 3-dimensional finite element approach. *PLoS ONE* **3**, e2200. (doi:10.1371/journal.pone.0002200)

Broom, R. 1947 Discovery of a new skull of the South African Ape-man, *Plesianthropus*. *Nature* **159**, 672. (doi:10.1038/159672a0)

Christiansen, P. & Wroe, S. 2007 Bite forces and evolutionary adaptations to feeding ecology in carnivores. *Ecology* **88**, 347–358. (doi:10.1890/0012-9658(2007)88[347:BFAEAT]2.0.CO;2)

Clausen, P., Wroe, S., McHenry, C., Moreno, K. & Bourke, J. 2008 The vector of jaw muscle force as determined by computer-generated three dimensional simulation: a test of Greaves' model. *J. Biomech.* **41**, 3184–3188. (doi:10.1016/j.jbiomech.2008.08.019)

Davis, J. L., Santana, S. E., Dumont, E. R. & Grosse, I. R. 2010 Predicting bite force in mammals: two-dimensional versus three-dimensional lever models. *J. Exp. Biol.* **213**, 1844–1851. (doi:10.1242/jeb.041129)

Demes, B. & Creel, N. 1988 Bite force, diet, and cranial morphology of fossil hominids. *J. Hum. Evol.* **17**, 657–670. (doi:10.1016/0047-2484(88)90023-1)

Dumont, E. R., Piccirillo, J. & Grosse, I. R. 2005 Finite-element analysis of biting behavior and bone stress in the facial skeletons of bats. *Anat. Rec. Part A* **283A**, 319–330.

Dumont, E. R., Grosse, I. R. & Slater, G. J. 2009 Requirements for comparing the performance of finite element models of biological structures. *J. Theoret. Biol.* **256**, 96–103. (doi:10.1016/j.jtbi.2008.08.017)

Ellis, J. L., Thomason, J. J., Kebreab, E. & France, J. 2008 Calibration of estimated biting forces in domestic canids: comparison of post-mortem and *in vivo* measurements. *J. Anat.* **212**, 769–780. (doi:10.1111/j.1469-7580.2008.00911.x)

Hylander, W. L., Johnson, K. R. & Crompton, A. W. 1992 Muscle force recruitment and biomechanical modeling: an analysis of masseter muscle function in *Macaca fascicularis*. *Am. J. Phys. Anthropol.* **88**, 365–387. (doi:10.1002/ajpa.1330880309)

Kupczik, K. & Dean, M. C. 2008 Comparative observations on the tooth root morphology of *Gigantopithecus blacki*. *J. Hum. Evol.* **54**, 196–2004. (doi:10.1016/j.jhevol.2007.09.013)

Kupczik, K., Dobson, C. A., Fagan, M. J., Crompton, R. H., Oxnard, C. E. & O'Higgins, P. 2007 Assessing mechanical function of the zygomatic region in macaques: validation and sensitivity testing of finite element models. *J. Anat.* **210**, 41–53. (doi:10.1111/j.1469-7580.2006.00662.x)

Leakey, L. S. B. 1959 A new fossil skull from Olduvai. *Nature* **184**, 491–493. (doi:10.1038/184491a0)

Lucas, P. W., Peters, C. R. & Arrandale, S. R. 1994 Seed-breaking forces exerted by orang-utans with their teeth in captivity and a new technique for estimating forces produced in the wild. *Am. J. Phys. Anthropol.* **94**, 365–378. (doi:10.1002/ajpa.1330940306)

Lund, J. & Kolta, A. 2006 Generation of the central masticatory pattern and its modification by sensory feedback. *Dysphagia* **21**, 167–174. (doi:10.1007/s00455-006-9027-6)

McCollum, M. A., Sherwood, C. C., Vinyard, C. J., Lovejoy, C. O. & Schachat, F. 2006 Of muscle-bound crania and human brain evolution: the story behind the MYH16 headlines. *J. Hum. Evol.* **50**, 232–236. (doi:10.1016/j.jhevol.2005.10.003)

McHenry, C. R., Wroe, S., Clausen, P. D., Moreno, K. & Cunningham, E. 2007 Supermodeled sabercat, predatory behavior in *Smilodon fatalis* revealed by high-resolution 3D computer simulation. *Proc. Natl Acad. Sci. USA* **104**, 16 010–16 015. (doi:10.1073/pnas.0706086104)

Nalla, R. K., Kinney, J. H. & Ritchie, R. O. 2003 Mechanistic failure criteria for the failure of human cortical bone. *Nat. Mat.* **2**, 164–168. (doi:10.1038/nmat832)

O'Connor, C. F., Franciscus, R. G. & Holton, N. E. 2005 Bite force production capability and efficiency in neanderthals and modern humans. *Am. J. Phys. Anthropol.* **127**, 129–151. (doi:10.1002/ajpa.20025)

Olejniczak, A. J., Tafforeau, P., Feeney, R. N. M. & Martin, L. B. 2008 Three-dimensional primate molar enamel thickness. *J. Hum. Evol.* **54**, 187–195. (doi:10.1016/j.jhevol.2007.09.014)

Preuschoft, H. & Witzel, U. 2002 Biomechanical investigations on the skulls of reptiles and mammals. *Senckenb. Lethaea* **82**, 207–222. (doi:10.1007/BF03043785)

Preuschoft, H. & Witzel, U. 2005 Functional shape of the skull in vertebrates: which forces determine skull morphology in lower primates and ancestral synapsids? *Anat. Rec. Part A* **283A**, 402–413.

Pruim, G. J., de Jongh, H. J. & ten Bosch, J. J. 1980 Forces acting on the mandible during bilateral static bite at different bite force levels. *J. Biomech.* **13**, 755–763. (doi:10.1016/0021-9290(80)90237-7)

Rayfield, E. J. 2005 Aspects of comparative cranial mechanics in the theropod dinosaurs *Coelophysis*, *Allosaurus* and *Tyrannosaurus*. *Zool. J. Linn. Soc. Lond.* **144**, 309–316. (doi:10.1111/j.1096-3642.2005.00176.x)

Rayfield, E. J., Norman, D. B., Horner, C. C., Horner, J. R., Smith, P. M., Thomason, J. J. & Upchurch, P. 2001 Cranial design and function in a large theropod dinosaur. *Nature* **409**, 1033–1037. (doi:10.1038/35059070)

Rohrle, O. & Pullan, A. J. 2007 Three-dimensional finite element modelling of muscle forces during mastication. *J. Biomech.* **40**, 3363–3372. (doi:10.1016/j.jbiomech.2007.05.011)

Sinn, D. P., De Assis, E. & Throckmorton, G. S. 1996 Mandibular excursions and maximum bite forces in patients with temporomandibular joint disorders. *J. Maxillofac. Surg.* **54**, 671–680.

Smith, J. M. & Savage, R. J. G. 1959 The mechanics of mammalian jaws. *School. Sci. Rev.* **40**, 289–381.

Stedman, H. H. *et al.* 2004 Myosin gene mutation correlates with anatomical changes in the human lineage. *Nature* **428**, 415–418. (doi:10.1038/nature02358)

Strait, D. S., Wang, Q., Dechow, P. C., Ross, C. F., Richmond, B. G., Spencer, M. A. & Patel, B. A. 2005 Modeling elastic properties in finite-element analysis: how much precision is needed to produce an accurate model? *Anat. Rec. Part A* **283A**, 275–287.

Strait, D. S. *et al.* 2009 The feeding biomechanics and dietary ecology of *Australopithecus africanus*. *Proc. Natl Acad. Sci. USA* **106**, 2124–2129. (doi:10.1073/pnas.0808730106)

Taylor, A. B. 2005 A comparative analysis of temporomandibular joint morphology in the African apes. *J. Hum. Evol.* **48**, 555–574. (doi:10.1016/j.jhevol.2005.01.003)

Thomason, J. J. 1991 Cranial strength in relation to estimated biting forces in some mammals. *Can. J. Zool.* **69**, 2326–2333. (doi:10.1139/z91-327)

Thomason, J. J., Russell, A. P. & Morgeli, M. 1990 Forces of biting, body size, and masticatory muscle tension in the oppossum *Didelphis virginiana*. *Can. J. Zool.* **68**, 318–324. (doi:10.1139/z90-047)

Thompson, D. W. 1917 *On growth and form*. Cambridge, UK: Cambridge University Press.

Tsafnat, N. & Wroe, S. In press. An experimentally validated micromechanical model of a rat vertebra under compressive loading. *Anat. Rec.* (JANAT-2010-0003, accepted 020210).

Vogel, E. R., Van Woerden, J. T., Lucas, P. W., Utami Atmoko, S. S., Van Schaik, C. P. & Dominy, N. J. 2008 Functional ecology and evolution of hominoid molar enamel thickness: *Pan troglodytes schweinfurthii* and *Pongo pygmaeus wurmbii*. *J. Hum. Evol.* **55**, 60–74. (doi:10.1016/j.jhevol.2007.12.005)

Walker, A. 1981 Dietary hypotheses and human evolution. *Phil. Trans. R. Soc. Lond. B* **292**, 57–64. (doi:10.1098/rstb.1981.0013)

Wall, C. E. 1999 A model of temporomandibular joint function in anthropoid primates based on condylar movements during mastication. *Am. J. Phys. Anthropol.* **109**, 67–88. (doi:10.1002/(SICI)1096-8644(199905)109:1<67::AID-AJPA7>3.0.CO;2-F)

Waugh, L. M. 1937 Influence of diet on the jaw and face of the American Eskimo. *J. Am. Dent. Assoc.* **24**, 1640–1647.

Wood, B. A. & Richmond, B. G. 2000 Human evolution: taxonomy and paleobiology. *J. Anat.* **196**, 19–60.

Wrangham, R. W., Jones, J. H., Laden, G., Pilbeam, D. & Conklin-Brittain, N. L. 1999 The raw and the stolen: cooking and the ecology of human origins. *Curr. Anthropol.* **40**, 567–594. (doi:10.1086/300083)

Wroe, S. 2008 Cranial mechanics compared in extinct marsupial and extant African lions using a finite-element approach. *J. Zool. (Lond.)* **274**, 332–339. (doi:10.1111/j.1469-7998.2007.00389.x)

Wroe, S., McHenry, C. & Thomason, J. 2005 Bite club: comparative bite force in big biting mammals and the prediction of predatory behaviour in fossil taxa. *Proc. R. Soc. B* **272**, 619–625. (doi:10.1098/rspb.2004.2986)

Wroe, S., Clausen, P., McHenry, C., Moreno, K. & Cunningham, E. 2007*a* Computer simulation of feeding behaviour in the thylacine and dingo as a novel test for convergence and niche overlap. *Proc. R. Soc. B* **274**, 2819–2828. (doi:10.1098/rspb.2007.0906)

Wroe, S., Moreno, K., Clausen, P., McHenry, C. & Curnoe, D. 2007*b* High resolution three-dimensional computer simulation of hominid cranial mechanics. *Anat. Rec. Part A* **290**, 1248–1255.

Wroe, S., Huber, D., Lowry, M., McHenry, C., Moreno, K., Clausen, P., Cunningham, E., Mason, D. & Summers, A. 2008 Three-dimensional computer analysis of white shark jaw mechanics: how hard can a great white bite? *J. Zool. (Lond.)* **276**, 336–342. (doi:10.1111/j.1469-7998.2008.00494.x)